A Zonally-Averaged Global Atmospheric Transport Model for Long-lived Trace Gases

Luke M. Western[1,2], **Scott D. Bachman**[3], **Stephen A. Montzka**[1], **Matt Rigby**[2]

[1]Global Monitoring Laboratory, National Oceanic and Atmospheric Administration, Boulder, CO, USA
[2]School of Chemistry, University of Bristol, Bristol, UK
[3]Climate and Global Dynamics Laboratory, National Center for Atmospheric Research, Boulder, CO, USA

Key Points:

- A user-friendly 2D global atmospheric transport model using reanalysis data and flux-gradient experiments alongside a 3D model.
- Improved representation of emissions over box models, focusing on quantifying greenhouse gases and ozone-depleting substances.
- An open-source model, which surpasses box models, and is applicable to diverse studies on emissions and chemical processes.

Corresponding author: Luke M. Western, `luke.western@bristol.ac.uk`

Abstract

We present a two-dimensional, zonally averaged global model of atmospheric transport named MALTA: Model of Averaged in Longitude Transport in the Atmosphere. It aims to be accessible to a broad community of users, with the primary function of quantifying emissions of greenhouse gases and ozone depleting substances with improved representation over widely used box models. The model transport is derived from meteorological reanalysis data and flux-gradient experiments using a three-dimensional transport model. Atmospheric sinks are prescribed loss frequency fields. The zonally averaged model simulates important large-scale transport features such as the influence on trace gas concentrations of the quasi-biennial oscillation and variations in inter-hemispheric transport rates. Stratosphere-troposphere exchange is comparable to a three-dimensional model and inter-hemispheric transport is slightly faster than both the three-dimensional model from which transport rates are derived and that estimated from measurements. Validation of the model shows that it outperforms a commonly used box model of atmospheric transport when used to derive emissions. The model is open source and is expected to be applicable to a wide range of studies requiring a fast, simple model of atmospheric transport and chemical processes for estimating associated emissions or mole fractions.

Plain Language Summary

We introduce a simplified global model that simulates the movement of gases in the atmosphere. The main goal of this model is to understand how greenhouse gases and substances that deplete the ozone layer are transported and distributed, and to more accurately estimate their global emissions using concentrations measured in the atmosphere over time. To achieve this, the model uses data from weather analysis and experiments conducted with a more complex three-dimensional model. The model calculates how gases move across different latitudes and altitudes, and accounts for their chemical loss. The simplified model can accurately reproduce large-scale atmospheric transport phenomena. The model is publicly available. We expect it to be useful for research that requires a fast and easy to use model to understand large-scale atmospheric transport and related processes.

1 Introduction

Supplying observation-based global emission estimates for long-lived gases is important for assessing the success of international policies designed to minimise these emissions and their environmental impacts. A prime example is the quadrennial Scientific Assessment of Ozone Depletion (World Meteorological Organization (WMO), 2022), which reports on emissions of ozone-depleting substances and other greenhouse gases of interest to the Montreal Protocol on Substances that Deplete the Ozone Layer. The Montreal Protocol controls production and consumption of ozone-depleting substances, and other greenhouse gases through the Kigali Amendment, and has been the driver behind ozone layer recovery and the avoidance of large-scale additional global warming (Newman et al., 2009). Global emissions for the majority of greenhouse gases and ozone depleting substances reported in the Scientific Assessment of Ozone Depletion were quantified using a well-established method, which uses measurements of atmospheric concentration near the Earth's surface coupled with a simple box model of global atmospheric transport in an inverse framework (e.g., Cunnold et al., 1983; Rigby et al., 2013). Simple models of atmospheric transport and loss, such as in a box model representation of the global atmosphere with annually repeating dynamics, have limitations. For example, features of large-scale dynamics, such as the quasi-biennial oscillation of the direction of the zonal wind in the tropical lower stratosphere (QBO), affect surface concentrations of trace gases, but cannot be represented in those models (Ray et al., 2020; Ruiz et al., 2021; Montzka

et al., 2021). Low spatial resolution in simple box models also leads to substantial representation errors, when point measurements are compared to simulations of concentrations in very large boxes. Such errors in modelled surface concentration are propagated into emissions estimates.

There is a need to improve the interpretation of temporal changes in atmospheric concentration measurements, to supply more accurate estimates of emissions on policy-relevant timescales, e.g., annually. For example, emissions of CFC-11, quantified using a box model with annually repeating mixing and advection, increased after their global phase-out (Montzka et al., 2018), most likely due to production that was not reported to the Montreal Protocol (Park et al., 2021). The initial box model emissions estimates were adjusted to account for variability in atmospheric dynamics using 3D models, revealing large uncertainties the derived emissions for some years (Montzka et al., 2021). However, this procedure of using a 3D model to correct for variability in atmospheric dynamics is complex and not readily available for other species. Therefore, to account for inter-annual variability in atmospheric dynamics, and reduce representation errors, there is a need to improve the modelling of atmospheric trace gases. Simultaneously, any transport modelling approach must be fast and simple to use, given the number of gases that must be quantified for reports such as the Scientific Assessment of Ozone Depletion, from multiple measurement networks, and interim scientific studies (e.g., Stanley et al., 2020; Mühle et al., 2022; L. M. Western et al., 2023). This makes quantifying emissions using established three-dimensional chemical transport models prohibitive, except for individual focused studies (e.g., Lunt et al., 2015; Claxton et al., 2020; Montzka et al., 2021). Here we describe a new zonally averaged two-dimensional model of global atmospheric transport that uses more representative transport, at higher resolution in space and time, than current box-modelling approaches, and considers time-varying large-scale dynamics.

Zonally averaged two-dimensional (2D) models of atmospheric transport have been widely used to study problems in the atmospheric sciences (Hough, 1989; Strand & Hov, 1993; Fleming et al., 2020). Here, we limit the term box model to simple low-resolution (1-12 regions for the entire globe) paramaterisations of zonally averaged transport and use the term 2D model to mean a zonally averaged model that attempt to provide a more rigorous representation of advective-diffusive processes. Many past studies using 2D models have focused on processes in the middle atmosphere (∼10-90 km), although a 2D model with annually-repeating transport has previously been used to quantify emissions of long-lived halocarbons (e.g., Newland et al., 2013; Laube et al., 2016; Adcock et al., 2018). The use of a zonally-averaged approach is generally justified for long lived trace gases given the zonal symmetry typically measured for their mole fractions in the background atmosphere, i.e., those measured far from emissions sources.

The new 2D model, named MALTA: Model of Averaged in Longitude Trasnport in the Atmosphere, is open-source and aims to be accessible to a broad community of users, with the primary function of quantifying emissions of greenhouse gases and ozone depleting substances with improved representation over current box models. The model and its components are written in the widely used Python programming language, which should help accessibility, compared to compiled languages. Performance is greatly improved over a standard Python implementation by exploiting just-in-time compilation (Lam et al., 2015). Section 2 details the derivation of the model transport parameters; section 3 describes the numerical schemes applied to solve model transport, source and sinks; section 4 presents some approaches to assess the performance of the model; and the concluding remarks are presented in section 5.

2 Derivation of zonally-averaged transport parameters

Zonally averaged transport characteristics of the atmosphere are paramaterised from three-dimensional meteorological fields and transport tendencies (see e.g., Plumb & Mahlman, 1987) for each calendar month from 1980 onward. Prior to 1980, the 2D model uses a monthly climatology (1980-2020) of the transport parameters. The model is in Cartesian coordinates, where y is the horizontal meridional coordinate of metres from the equator, defined as

$$y = R\phi, \tag{1}$$

where R is the radius of Earth and ϕ is latitude in radians. The vertical component z is a scale-height

$$z = H \ln\left(\frac{p_s}{p}\right), \tag{2}$$

where p is zonally averaged atmospheric pressure, $H = 7200$ km and $p_s = 1000$ hPa. The horizontal (y) resolution is every 10° in latitude and the bounds of altitude (z) are at 30 levels (29 layers) spaced equally in log-pressure coordinates between 1000 and 10 hPa (approximately 1150m).

No topography is present in the 2D model, and thus there is no explicit parameterisation of phenomena such as topography-induced gravity waves. Explicit parameterisation of localised phenomena such as convection are also neglected (see e.g., Strand and Hov (1993) for a zonally-averaged implementation of convection). The choice of Cartesian coordinates has been made for their relative simplicity over more complex, but perhaps better surface-resolving coordinate systems (see, e.g., Tung, 1982; Iwasaki, 1989).

By denoting a zonal-temporal average by an overbar and a prime as the deviation from this average, the zonally averaged budget equation for a trace gas with an atmospheric mole fraction q is,

$$\frac{\partial \bar{q}}{\partial t} = \bar{s} - \bar{\mathbf{u}} \cdot \nabla \bar{q} - \nabla \cdot \overline{\mathbf{u}'q'}, \tag{3}$$

where v is the north-south wind velocity and w is the upward wind velocity $\big($we define $\mathbf{u} = (v, w)\big)$, and s represents the sources and sinks. The derivative $\nabla = \frac{\partial}{\partial y} + \frac{\partial}{\partial z}$. Here $\overline{\mathbf{u}'q'}$ is an eddy-flux term, which we expand on in the following section.

2.1 The zonally averaged flux-gradient relationship

The eddy-flux term $\overline{\mathbf{u}'q'}$ from equation 3 can be paramterised as

$$\overline{\mathbf{u}'q'} = -\mathbf{K} \cdot \nabla \bar{q}, \tag{4}$$

where $\mathbf{K}$ is a 2×2 eddy transport tensor,

$$\mathbf{K} = \begin{bmatrix} K_{yy} & K_{yz} \\ K_{zy} & K_{zy} \end{bmatrix}.$$

The eddy transport tensor can be expressed as the sum of a symmetric diffusive tensor, $\mathbf{D}$, and antisymmetric advective tensor, $\mathbf{A}$, (Plumb, 1979; Griffies, 1998; S. D. Bachman et al., 2020),

$$\mathbf{A} = \frac{1}{2}\left(\mathbf{K} - \mathbf{K}^T\right) \tag{5a}$$

$$\mathbf{D} = \frac{1}{2}\left(\mathbf{K} + \mathbf{K}^T\right). \tag{5b}$$

This allows the flux-gradient relationship in equation 4 to be rewritten,

$$\overline{\mathbf{u}'q'} = -\mathbf{K} \cdot \nabla \bar{q} \tag{6a}$$

$$= -(\mathbf{A} + \mathbf{D}) \cdot \nabla \bar{q} \tag{6b}$$

$$= -\begin{bmatrix} 0 & \psi \\ -\psi & 0 \end{bmatrix} \cdot \nabla \bar{q} - \begin{bmatrix} D_{yy} & D_{yz} \\ D_{zy} & D_{zz} \end{bmatrix} \cdot \nabla \bar{q}, \tag{6c}$$

where ψ is the streamfunction for zonally-averaged coordinates. Following this approach, the eddy-induced advection v^* and w^* is derived (Griffies, 1998) following

$$v^* = \frac{\partial \psi}{\partial z}, \tag{7a}$$

$$w^* = -\frac{\partial \psi}{\partial y}, \tag{7b}$$

and the eddy-induced diffusion terms are taken directly from the tensor components of $\mathbf{D}$ from equation 5, i.e.,

$$D_{yy} = K_{yy}, \tag{8a}$$

$$D_{zz} = K_{zz}, \tag{8b}$$

$$D_{yz} = D_{zy} = \frac{1}{2}\left(K_{yz} + K_{zy}\right). \tag{8c}$$

Substituting this flux-gradient relationship into equation 3 gives the continuity equation in terms of a residual velocity and eddy-induced diffusion,

$$\frac{\partial \bar{q}}{\partial t} = \bar{s} - (\bar{v} + v^*)\frac{\partial \bar{q}}{\partial y} - (\bar{w} + w^*)\frac{\partial \bar{q}}{\partial z} + \nabla \cdot (\mathbf{D} \cdot \nabla \bar{q}). \tag{9}$$

Alternate derivations of residual circulation exist (see e.g., Holton, 1981; Andrews et al., 1999).

2.2 Tracer-based estimates of eddy transport

To estimate the components of $\mathbf{K}$ we follow the approach of S. Bachman et al. (2015). The idea is to use the eddy-flux term in equation 4 to estimate

$$\mathbf{K} = -\overline{\mathbf{u}'q'}\left(\nabla \bar{q}\right)^T \left(\left(\nabla \bar{q}\right)^T \nabla \bar{q}\right)^{-1}. \tag{10}$$

Tracer experiments from a three-dimensional model provide the information to diagnose 2D transport (Plumb & Mahlman, 1987). We choose to use six sinusoidally orthogonal pairs of tracer fields (varying in y and $\log(z)$) to initialise the model (following S. Bachman & Fox-Kemper, 2013, Appendix B). The tracers are inert (with a molar mass nominally equal to carbon monoxide) and have no emission source. The experiments are run using the GEOS-Chem transport model (Bey et al., 2001; The International GEOS-Chem User Community, 2021) driven by MERRA-2 reanalysis meteorology (Gelaro et al., 2017) at $4^\circ \times 5^\circ$ spatial resolution from 1980 onward. Each tracer field is run for one month from the initialised state to infer the mean zonally-averaged eddy-transport for that month, and the three-dimensional tracer and meteorological fields are output every minute.

We derive the eddy-transport by first interpolating the three-dimensional fields onto the two-dimensional vertical and latitudinal resolution at each time step using bilinear interpolation (Zhuang et al., 2020). We infer the tensor $\mathbf{K}$ using the tensor of tracer fields $\mathbf{q}$ using an approach akin to maximum likelihood estimation, where i and j are an index of the vertical and horizontal grid cells, by

$$(K_{yy}, K_{yz})_{ij} = -\left(\overline{v'\mathbf{q}'}\right)_{ij} \mathbf{P}_{ij}^{-1} \left(\nabla \overline{\mathbf{q}}\right)_{ij}^T \left(\left(\nabla \overline{\mathbf{q}}\right)_{ij} \mathbf{P}_{ij}^{-1} \left(\nabla \overline{\mathbf{q}}\right)_{ij}^T\right)^{-1} \tag{11}$$

and

$$(K_{zy}, K_{zz})_{ij} = -\left(\overline{w'\mathbf{q}'}\right)_{ij} \mathbf{P}_{ij}^{-1} \left(\nabla \overline{\mathbf{q}}\right)_{ij}^T \left(\left(\nabla \overline{\mathbf{q}}\right)_{ij} \mathbf{P}_{ij}^{-1} \left(\nabla \overline{\mathbf{q}}\right)_{ij}^T\right)^{-1}. \tag{12}$$

The square matrix $\mathbf{P}_{ij}$ is a diagonal weighting matrix,

$$\mathbf{P}_{ij} = \mathrm{Diag}\left(\mathbf{q}_{ij}(\mathbf{1}^T \mathbf{q}_{ij})^{-1}\right)$$

where **1** is a column vector of ones (similar to, e.g., Bratseth, 1998; S. Bachman et al., 2015).

Some quality control following Plumb and Mahlman (1987) is placed on the derived diffusion parameters. That is, D_{yy} (which is equal to K_{yy}) was set to a minimum value of $10^4 \cos^2 \phi$ m^{2}s^{-1}, and we ensure that $D_{yz}^2 \leq D_{zz} D_{yy}$ (ensure antidiffusion is not possible) by adjusting D_{zz} accordingly. Finally, based on comparisons with the zonal average of tracer experiments using GEOS-Chem, values in D_{zz} were adjusted upwards by 50% and values of D_{yz} down by 25%, which gave a better overall fit to the 3D modelled tracer fields.

2.3 Advective fields

The advective fields are taken as zonal and monthly averages from MERRA-2 reanalysis for each year, and combined with the eddy-induced residual advection (Section 2.1) to create a single advective field. Following interpolation and averaging, the 2D advective fields become divergent. We address this problem by adjusting the vertical velocity $\overline{w}+w^*$ following Shine (1989) to ensure that the area-averaged vertical velocity is zero, i.e., in each layer i additively adjust $\overline{w}_i + w_i^*$ by a factor of

$$\xi_i = -\frac{\int_{-\frac{\pi}{2}}^{\frac{\pi}{2}} (\overline{w}_i + w_i^*) \cos\phi \, d\phi}{\int_{-\frac{\pi}{2}}^{\frac{\pi}{2}} \cos\phi \, d\phi}, \tag{13}$$

to ensure that

$$\int_{-\frac{\pi}{2}}^{\frac{\pi}{2}} (\overline{w}_i + w_i^*) \cos\phi \, d\phi = 0. \tag{14}$$

Using the adjusted values for $\overline{w} + w^*$, we compute the non-divergent values for $\overline{v} + v^*$ by ensuring mass balance during advection between grid cells.

3 Computation of model processes

The parameters derived in Section 2 transport the mixing ratio of the trace gas following equation 9. The transport, source and sink processes are broken down using time splitting. Initially, at time t, the tracer is emitted into the atmosphere (generally in the lowest layer of the model). Following this, at time $t+\tau_1$, the field is advected using the residual velocity (Section 3.1). At time $t+\tau_2$, diffusion occurs in the y and z direction using the diagonal of the eddy-diffusion tensor (using D_{yy} and D_{zz}, Section 3.2), followed by the off-diagonal eddy diffusion component at time $t+\tau_3$ (Section 3.2.1). Finally at time $t + \tau_4$, any atmospheric sink is imposed (Section 3.3). The numerical implementation of these approaches is described in the following subsections.

3.1 Advection

The advection scheme is based on Lin and Rood (1996). The scheme conserves mass, a uniform concentration field, is positive definite, ensures monoticity and is numerically efficient. The tracer field is advected using the residual velocities $\bar{v} + v^*$ and $\bar{w} + w^*$ and computed on an Arakawa C-grid (Arakawa & Lamb, 1977). A monoticity constraint on the upwind fluxes is imposed following equation 5 in Lin et al. (1994), meaning that a monotonic mixing ratio gradient before advection will maintain this monotonic distribution after advection. The fractional fluxes in the Lin and Rood (1996) scheme are computed using the Piecewise Parabolic Method (PPM, Colella & Woodward, 1984). Note that, given the parameters in Section 2 and a time step of around 8 hours, the Courant number does not exceed one and so the semi-Lagrangian component presented in Lin and

Rood (1996) is not needed. Over and undershoots are eliminated using the first constraint proposed in Appendix C of Lin and Rood (1996), where edge values are computed following Carpenter et al. (1990). Finally, fluxes between grid cells are computed following Colella and Woodward (1984). See the supplementary information for a more detailed description of the steps and equations used.

3.2 Diffusion

Diffusion is controlled through the diffusion tensor $\mathbf{D}$, Section 2.1. We solve the diffusion due to the diagonal of the eddy-diffusion tensor (D_{yy} and D_{zz}) using an Eulerian approach on an Arakawa C-grid (Arakawa & Lamb, 1977). Diffusion is calculated using second-order central finite difference in the vertical and horizontal. We use a Runge–Kutta, or RK4, method for the temporal discretisation (e.g., Butcher, 1996).

While finite difference methods are sufficient for diffusion from the diagonal of the eddy diffusion tensor, the off-diagonal elements need more detailed treatment.

3.2.1 Mixed derivative diffusion

Mixed derivative second order finite difference methods are not generally positivity-preserving, which is necessary for the transport of atmospheric trace gases. Therefore, the Eulerian approach applied to the diagonal elements of the eddy diffusion tensor cannot be applied to the off-diagonal elements. Instead, we adapt the approach proposed by du Toit et al. (2018) to ensure positive definite tracer concentrations following the diffusion terms containing a mixed derivative.

The idea is to reframe the mixed-derivative diffusion processes as advective processes that can be solved using a positivity-preserving scheme, as in Section 3.1. Diffusion using the D_{yz} component can be written,

$$D_{yz}\frac{\partial^2 \overline{q}}{\partial y \partial z} = v_d \frac{\partial \overline{q}}{\partial y}, \tag{15}$$

where

$$v_d = \frac{D_{yz}}{\overline{q}}\frac{\partial \overline{q}}{\partial z}, \tag{16}$$

and equation 15 takes a similar form to the advective terms in equation 9. The $\frac{\partial \overline{q}}{\partial z}$ term in equation 16 can be solved using standard second order central finite difference methods. However, following equation 16, as $\overline{q} \to 0, v_d \to \infty$. We therefore impose the limit that $v_d = 0$ when $\overline{q} < \epsilon$, where ϵ is around five orders of magnitude less than the expected surface concentration of the tracer. Conceptually, this implies that the diffusion tensor is diagonal for small concentrations. The same approach is taken for the corresponding w_d for diffusion using the D_{zy} component.

The terms v_d and w_d are calculated using an Arakawa A-grid (Arakawa & Lamb, 1977), but the advection scheme in Section 3.1 requires an Arakawa C-grid. The transport scheme therefore requires interpolation of v_d and w_d onto the Arakawa C-grid using linear interpolation. These advective-like terms are then used as described in Section 3.1 to advect, and therefore diffuse, the tracer field.

3.3 Sinks

An explicit chemistry scheme is not currently implemented in the model. Loss due to reaction with the hydroxyl radical (OH) is calculated using the Arrhenius equation, with reaction rates taken from J. Burkholder et al. (2020) and temperatures taken from the MERRA-2 reanalysis. The OH fields were taken from Pimlott et al. (2022) using their values derived for 2010, with different OH fields (concentration and distribution) applied

for each month, which were zonally averaged and scaled, by the same constant value in space and for each month, to the tropospheric lifetime, or lifetime due to OH reactive loss, of methyl chloroform (6.1 years, J. B. Burkholder & Hodnebrog, 2022).

Stratospheric sinks due to photolysis and reaction with excited oxygen (O^1D) are calculated using a first order loss frequency field (the inverse of the local lifetime in each grid cell), taken from zonally averaged loss fields in the climatological stratosphere (driven by the MERRA-2 reanalysis) from prior 3D model simulations (e.g., Murray et al., 2012). We assume that only loss due to OH occurs in the troposphere. Given the tropospheric lifetime, we tune the stratospheric lifetime such that the total atmospheric lifetime is equal to that reported in J. B. Burkholder and Hodnebrog (2022), unless another desired lifetime is needed, by summing the inverse lifetimes in the troposphere and stratosphere. The atmospheric lifetime is estimated when the target species is in near-steady state in the atmosphere, following a 20-year spin-up period. These loss frequencies vary by month but repeat annually.

4 Model performance

In this section we evaluate the performance of the model. In section 4.1 we compare mole fractions of the atmospheric tracer sulphur hexafluoride (SF_6) modelled using the 2D model to those from GEOS-Chem, which was used to derive the eddy-transport tensors, and a 12-box model. Where we compare atmospheric concentrations at a particular altitude, the scale-height in the 2D model is treated as metres above sea-level (masl). Section 4.2 evaluates the timescales of inter-hemispheric transport of the 2D model compared to GEOS-Chem and estimated from observations, and section 4.3 evaluates the stratosphere-troposphere exchange, using SF_6 as a tracer. Section 4.4 assesses the ability of the 2D model to represent the influence of the QBO on atmospheric mole fractions of CFC-11, and discusses some the observed features. We derive emissions of CFC-11 in Section 4.5 using modelled mole fractions from a distinct 3D transport model with a known emissions input.

4.1 Modelled surface mole fractions

Here we compare modelled surface mole fractions of SF_6 taken from the 2D model to those output from the 3D model GEOS-Chem. In addition, we compare compare these surface mole fractions to those modelled using a 12-box model (Cunnold et al., 1983; Rigby et al., 2013). We model SF_6 as a tracer with an infinite lifetime (in the 2D model, GEOS-Chem and the 12-box model) to assess only the transport within the model. Emissions are from the EDGAR v4.2 emissions inventory (Janssens-Maenhout et al., 2011). Emissions are assumed to be constant in each calendar year. Note that the initial conditions in 1980 are somewhat higher than those from atmospheric measurements (Simmonds et al., 2020).

The 2D model and GEOS-Chem simulated mole fractions generally agree well. The 2D model's performance is improved over the 12-box model when compared to the grid cells in GEOS-Chem containing 12 measurement sites in the National Oceanic and Atmospheric Administration's (NOAA) measurement network (ALT, Alert, Canada, 82.5°N, 185 masl; SUM, Summit, Greenland, 72.6°N, 3210 masl; BRW, Barrow, Alaska, 71.3°N, 11 masl; MHD, Mace Head, Ireland, 53.3°N, 5 masl; THD, Trinidad Head, California, 41.1°N, 107 masl; NWR, Niwot Ridge, Colorado, United States, 40.1°N, 3523; KUM, Cape Kumukahi, Hawaii, 19.5°N, 8 masl; MLO, Mauna Loa, Hawaii, 19.5°N, 3397 masl; SMO, Cape Matatula, American Samoa, 14.2°N, 82 masl; CGO, Cape Grim, Tasmania, 40.7°N, 94 masl; PSA, Palmer Station, Antarctica, 64.9°N, 10 masl; and SPO, South Pole, Antarctica, 90.0°N, 2810 masl). Figure 1 shows a comparison of the modelled monthly mean SF_6 surface mole fraction simulated using the 2D model, GEOS-Chem and the 12-box model between 1980-2008 at four site locations: NWR, MLO, SMO and SPO. When com-

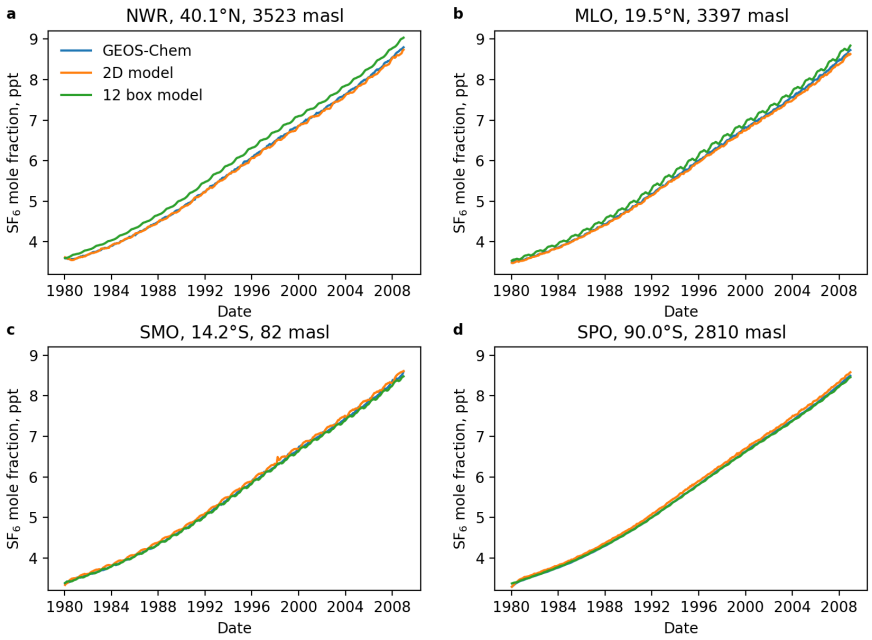

Figure 1. A comparison of the modelled mole fraction at the grid cells containing four measurement sites using GEOS-Chem, the 2D model and a 12-box model. The four represented measurement sites are given by their three letter acronym, and are (a) Niwot Ride, Colorado, USA, (b) Mauna Loa, Hawaii, USA, (c) Tutuila, American Samoa, and (d) South Pole, Antarctica.

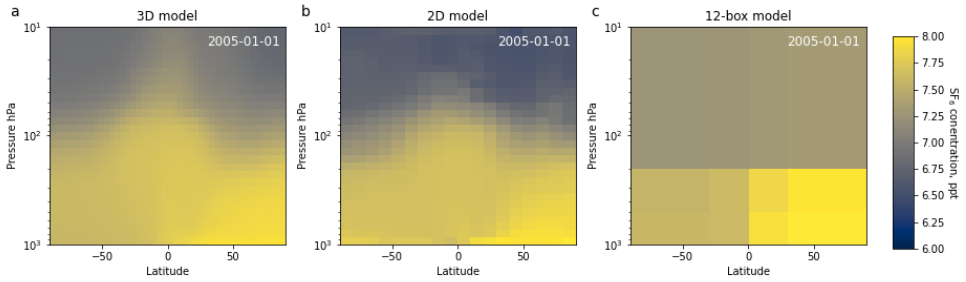

Figure 2. The monthly mean mole fraction from (a) the zonal average of a 3D model (GEOS-Chem), (b) the 2D model and (c) 12-box model for January 2005 for the emissions scenario described in Section 4.1.

pared to GEOS-Chem, the root-mean-squared error of the mole fraction over all sites for the 2D model is 0.08 ppt, compared to 0.11 ppt for the box model, and this error grows over time for both the 2D and 12-box model. The bias in the 2D model is -0.05 ppt for all sites compared to -0.08 ppt in the 12-box model. The 2D model does not outperform the 12-box model at every site, with the 2D model slightly overestimating the mole fractions in the Southern Hemisphere compared to GEOS-Chem and the 12-box model, most likely due to the faster inter-hemispheric transport time in the 2D model (see section 4.2). Coarsening of the model spatial resolution is known to increase errors in transport (Yu et al., 2018), which, along with coarsening of the temporal resolution, may explain some of the discrepancies between the models. Figure 2 shows the monthly mean mole fraction for January 2005 of the 12-box model, 2D model and the zonal average of GEOS-Chem throughout the atmosphere, demonstrating the difference in their horizontal and vertical resolution and simulated mole fractions.

4.2 Inter-hemispheric transport

We evaluate the inter-hemispheric transport of GEOS-Chem and the 2D model using two metrics: the age of air of SF_6 between the northern and southern hemisphere mean surface mole fractions (Waugh et al., 2013) and the inter-hemispheric exchange time, τ_{ex} (Patra et al., 2009) using the model runs described in Section 4.1. In addition, we present the age of air and τ_{ex} derived using hemispheric averaged SF_6 measurements from 1996 through 2008 made as part of the NOAA Global Monitoring Laboratory air sampling network (Dutton et al., 2022). We follow a similar approach to Yang et al. (2019) when evaluating these metrics. The age of air of SF_6 (a_{SF_6},the time lag for the mean mole fraction in the southern hemisphere to equal that in the northern hemispheric), is calculated as,

$$q_{\text{SH}}(t) = q_{\text{NH}}\left(t - a_{\text{SF}_6}\right), \tag{17}$$

where t is time, q is the average mole fraction in the northern and southern hemisphere, denoted by its subscripts. The inter-hemispheric exchange time is,

$$\tau_{\text{ex}} = \frac{\left(q_{\text{NH}} - q_{\text{SH}}\right)\left(\frac{E_{\text{NH}}}{E_{\text{SH}}} + 1\right)}{\frac{E_{\text{NH}}}{E_{\text{SH}}}\frac{\mathrm{d}q_{\text{SH}}}{\mathrm{d}t} - \frac{\mathrm{d}q_{\text{NH}}}{\mathrm{d}t}}, \tag{18}$$

where E is the emissions in each hemisphere. We use all available northern and southern hemisphere measurement data from the sites described in Section 4.1 in the calculation of the metrics, unlike in e.g., Yang et al. (2019), and therefore restrict the model runs to the dates of available measurements at the locations of the measurement sites described in 4.1. As in Yang et al. (2019), the age of air is calculated using 23-month

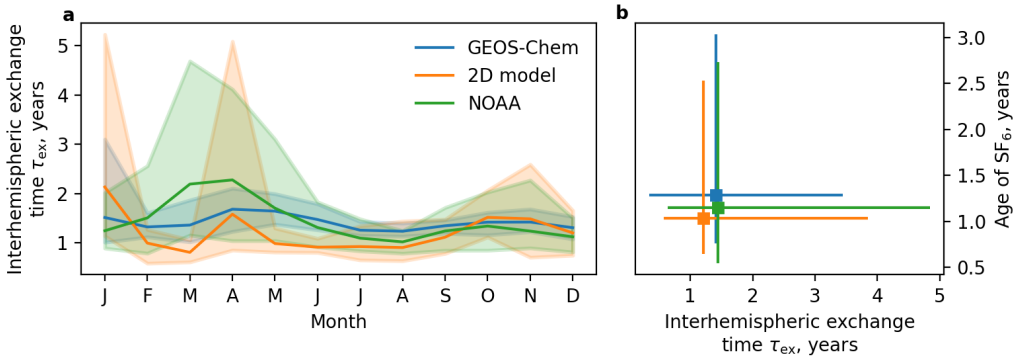

Figure 3. A comparison of the north to south transport timescale of SF_6 using GEOS-Chem, the 2D model and derived from measurements from the NOAA network, 1996-2008. (a) The mean seasonal pattern of the interhemispheric exchange time, τ_{ex}, of SF_6. Shading shows the 95% percentile for each month. (b) A comparison of τ_{ex} and the age of SF_6, where the squares show the mean monthly-derived values over 1996-2008 and lines extend to the 95% percentile.

smoothed mole fractions (using a 23-month exponentially-weighted moving window) for each site, for both the model runs and the measurements.

Note that the modelled mole fractions are not meant to be representative of the truth in this scenario. Instead, we assume that the hemispheric distribution of emissions from EDGAR v4.2 are sufficiently representative of the true emissions distribution to make a meaningful qualitative comparison between the models and measurements. Here we do not discuss the inter-hemispheric transport in the 12-box model as the transport is prescribed and annually repeating.

Figure 3(b) shows the mean age of air of SF_6 between the northern and southern hemispheres and τ_{ex}. The mean age of air is younger in the 2D model (1.0 years) than in GEOS-Chem (1.3 years). The age of air derived from observations falls in between the 2D model and GEOS-Chem (1.2 years). When considering the distribution of age of air values between the models and measurements, there is no clear indicator to whether the age of SF_6 is younger in the 2D model or derived from measurements, given the skew of the distributions. Both the 2D model and measurement-derived ages are younger than that of GEOS-Chem.

Also in figure 3(b) is the mean τ_{ex}. The 2D model has a faster exchange time (1.2 years) than GEOS-Chem and that derived from measurements (1.4 years), as was the case for the age of air SF_6 metric. The skewed distributions of τ_{ex} show that some of the longest τ_{ex} monthly values are derived from measurements, and the shortest from GEOS-Chem.

The mean annual cycle of τ_{ex} for each month is also shown in Figure 3. The age of air of the 2D model is generally younger (exchange is faster) than both GEOS-Chem and that derived from measurements in the period April-June. The models' and the measurement derived transport generally agree for the rest of the year. The 2D model has oldest age of air in the northern hemisphere autumn and winter months, which contrasts with GEOS-Chem and that derived from measurements, which have the oldest age of air during the northern hemisphere spring.

The cause of the differences of the transport seasonality in the 2D model, compared to GEOS-Chem and the measurements, during April-June is unclear. The reason for the

differences between the seasonal cycles in GEOS-Chem and the 2D model may come from the zonal averaging of the parameters within the model, for example where the distribution of the zonal transport is strongly non-normal. The transport processes controlling inter-hemispheric transport is known to be largely due convective processes, in particularly in tropical and sub-tropical latitudes (Gilliland & Hartley, 1998; Lintner et al., 2004; Patra et al., 2009). The 2D model does not explicitly parameterise convection. The lack of convective processes in the 2D model, which are known to largely impact transport timescales, may go some way to explain the discrepancy in interhemispheric transport (Orbe et al., 2018). Two-dimensional zonally-averaged parameterised convection has previously been implemented (Strand & Hov, 1993), however the applicability of a zonal average to represent convective processes is unclear, as they are regionally localised. Regional, longitudinally dependent convective processes can modulate interhemispheric transport (Lintner et al., 2004), which are clearly neglected in the 2D model given the lack of any longitudinal variations. For example, the Indian Ocean Monsoon, and strengthening of convection along the Indian Ocean Intertropical Convergence Zone, is known to modulate interhemispheric transport during the Northern Hemisphere summer (Lintner et al., 2004). This may indicate a shortcoming in the 2D in representing interhemispheric transport dominated convective process, over the advective dominated processes in extratropical latitudes (Patra et al., 2009). Despite the shortcomings surrounding the representation of convective processes in the 2D model, the 2D model generally performs well.

The lack of convective processes in the 2D model may have further implications for modelling of gases which can be rapidly transported into the upper troposphere - lower stratosphere by convective processes. This will be particularly pertinent for short-lived ozone-depleting substances (lifetime <6 months) where large emissions sources are co-located within the Asian monsoon region, e.g., (Adcock et al., 2021), and may mean that this model will introduce additional errors when studying these gases.

4.3 Stratosphere-troposphere exchange

We calculate the stratosphere-troposphere exchange (STE) of SF_6 from 1980-2008 between GEOS-Chem and the 2D model using the emissions scenario described in Section 4.1. For both models the location of the tropopause is taken from MERRA-2 reanalysis, based a minimum in the lapse rate, and we define the troposphere as all grid cells below the grid cell containing the tropopause. As SF_6 is modelled as having an infinite lifetime, we define stratosphere-troposphere exchange, $F_{S\rightarrow T}$, as

$$F_{S\rightarrow T} = \frac{dB_T}{dt} - E, \tag{19}$$

where the subscripts S and T denote the stratosphere and troposphere, B is the burden and E is the emissions to the troposphere per unit time.

Figure 4 shows a comparison of the STE of SF_6 from 1980-2008 between the two models. Both models exhibit an average STE maximum in June and a minimum in October, in line with current understanding (Appenzeller et al., 1996). The mean absolute magnitude of the STE is slightly larger in the 2D model than GEOS-Chem (4.2 vs 3.5 Gg yr^{-1}), and GEOS-Chem has, on average, slightly higher transport into the troposphere than the 2D model (overall mean STE of -0.7 Gg yr^{-1} for the 2D model vs -0.8 Gg yr^{-1} for GEOS-Chem). These differences are very small compared to the amplitude of the seasonal cycle of STE ($\sim$ 10 Gg yr^{-1}). It should be noted that GEOS-Chem is known to underestimate STE compared to some other transport models (Hu et al., 2017).

4.4 The quasi-biennial oscillation

A large motivation for the development and use of a 2D model over existing box models is to include features of large-scale dynamics and their interannual variability. The QBO has been shown to influence concentrations of trace gases at the surface, in

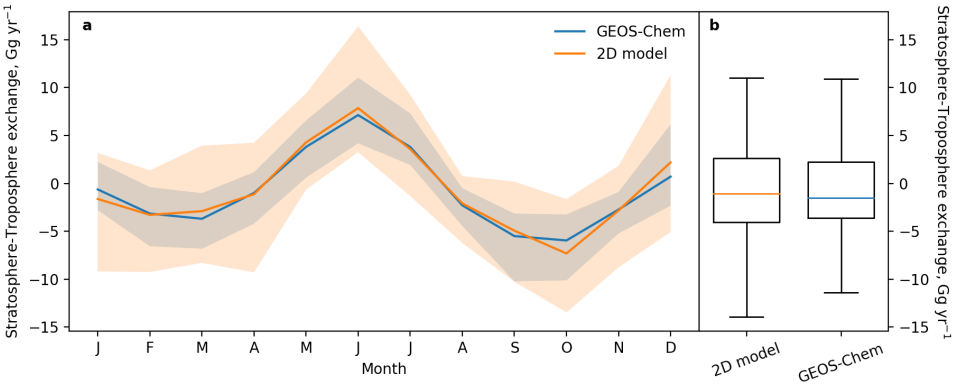

Figure 4. A comparison of the stratosphere-troposphere exchange of SF_6 from 1980-2008 between GEOS-Chem and the 2D model using the same emissions. (a) The monthly mean stratosphere-troposphere exchange between 1980-2008, where the shading shows the 95% variability. (b) Box plots show the median, interquartile range and 1.5× the interquartile range of the stratosphere-troposphere exchange.

particular of the long lived trace gas CFC-11 (Ray et al., 2020; Montzka et al., 2021; Ruiz et al., 2021).

We assess the 2D model representation of the QBO using transport of CFC-11, using an average lifetime of 52 years, tuned from an initial 3D field from Murray et al. (2012). Emissions to the 2D model are held constant at 88 Ggyr^{-1} following a 50 year spin up period (using approximate emissions from Laube et al. (2023)), which provides a near-steady state.

Figure 5 shows the latitudinally averaged partial pressure anomaly of CFC-11 in the 2D model as a function of time between 1990 and 2020 (see e.g., Ray et al., 2020). The anomaly has been filtered using a Butterworth bandpass filter of 22 to 34 months, where the mean QBO period is around 28 months (Baldwin et al., 2001). The QBO-induced partial pressure anomaly can generally be seen to propagate from the stratosphere down to the surface. There is a clear disruption in the signal around 2016, following an anomalous QBO phase (Newman et al., 2016). To a lesser degree there is some non-continuous propagation of the signal downwards from the stratosphere during the mid-1990s to 2000. Figure 5 shows the east-west equatorial wind anomaly at 20 hPa (filtered in the same way as the partial pressure anomaly), where the winds have been taken from ERA5 global reanalysis (Hersbach et al., 2020) in order to compare against an independent dataset. The phase of the east-west stratospheric wind anomaly at 20 hPa agrees well with the phase of the partial pressure anomaly at 20 hPa, which demonstrates that the model appears to qualitatively represent a QBO-induced anomaly well.

4.5 Estimation of modelled emissions

One of the primary foreseen uses of the new 2D model is to derive emissions of trace gases. Here, we demonstrate this use case by estimating emissions of CFC-11. As emissions are not known exactly in reality, we instead choose to use 3D-model-generated mole fractions, based on an emission history derived from a simple analysis of atmospheric measurements at remote sites across the globe (Montzka et al., 2021). We estimate emissions using modelled mole fraction output from the Whole Atmosphere Community Climate Model (WACCM, Marsh et al., 2013), which is independent of the GEOS-Chem model

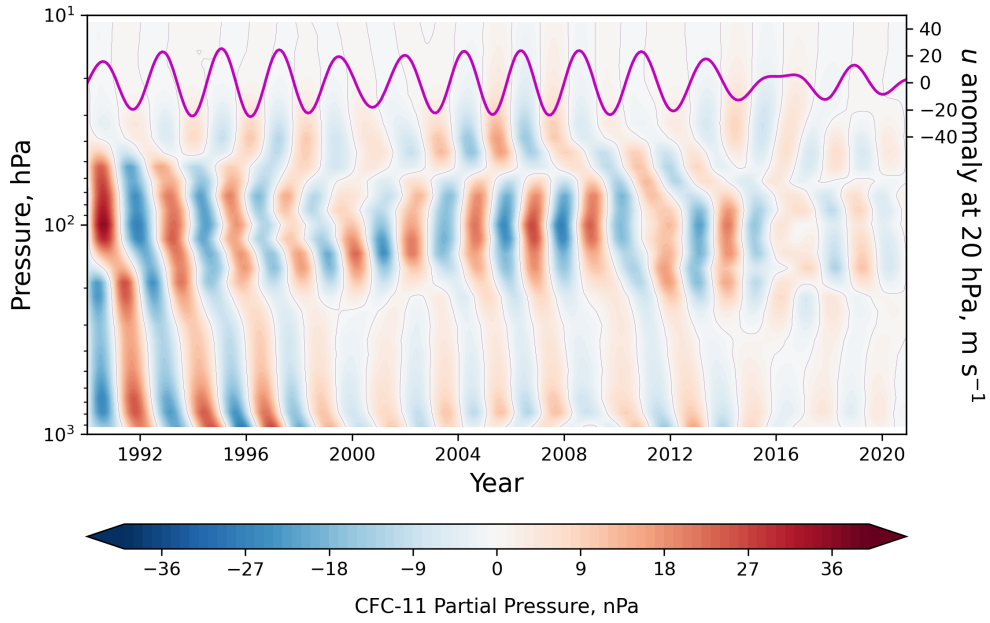

Figure 5. The global average partial pressure anomaly of CFC-11 in the 2D model due to the influence of the QBO is shown by the shading. The magenta line shows the east-west equatorial wind anomaly at 20 hPa.

used to derive the eddy-flux transport, although is also driven by MERRA-2 meteorology. Emissions used to generate the mole fraction are the smoothed emissions described in Montzka et al. (2021), and are distributed uniformly over all land areas.

The mole fractions used to estimate emissions were the monthly mean model 3D-output at the location of 12 measurement sites in NOAA's global monitoring network, which spans from -90.0°S to 82.5°N (see Section 4.1). The initial conditions for the mole fraction in the 2D model were estimated following a 50 year model spin-up which was then scaled to approximate that of the simulated measurement minus half the difference in the mole fraction between the first and second month of the WACCM output. Emissions were estimated between 1990-2019. The loss frequencies in the 2D model were scaled to yield a total atmospheric lifetime for CFC-11 of 56 years in order to match that of the mean global lifetime of CFC-11 in WACCM, using pre-calculated loss fields (Section 3.3).

To estimate annual emissions of CFC-11 from simulated mole fractions, we follow a Bayesian inverse framework, assuming a normal likelihood and prior distribution. Under the assumption of normality, an analytical solution can be found (see e.g., Tarantola, 2005). Emissions are assumed to be constant in each calendar year (they vary monthly in the WACCM simulation) and we infer emissions for each 10°latitude band. The prior mean emissions are random normal perturbations around the WACCM annual emissions, using a standard deviation of 10 Gg yr^{-1}. We then assign a one standard deviation uncertainty of 20 Gg yr^{-1} on the prior distribution in each latitude band. The likelihood assumes a combined model-measurement error of 5 ppt. Both the likelihood and prior distribution are assumed to be identical and independently distributed.

We also compare the estimated emissions using the 2D model to those estimated using a 12-box model using the same analytical inverse framework. The prior mean emissions are again random values about the annual emissions used within WACCM with a standard deviation of 10 Gg yr^{-1}, with a one standard deviation uncertainty of 20 Gg yr^{-1}. The measurements located in each of the four surface boxes are again given a 5 ppt one-standard deviation model-measurement error.

Figure 6 shows the estimated CFC-11 emissions derived from the WACCM simulated mole fractions. The 2D model-derived emissions agree with the emissions input to WACCM well. We do not display emissions in 1990 and 1991, the first year and second of the inversion, to allow the 2D model and box model to adjust any incorrect representation of the initial condition of mole fraction under the imposed statistical model.

Mean emissions derived using a 12-box model are less accurate than those derived using the 2D model (see Supplementary Information Figure S1). The posterior uncertainties in the 12-box model are also larger than those from the 2D model. The emissions used in WACCM to generate the mole fractions fall within the one standard deviation uncertainty of the emissions derived using the 12-box model for all years shown, except 1992.

5 Conclusions

We have presented a 2D zonally averaged global model of atmospheric transport named MALTA, Model of Averaged in Longitude Transport in the Atmosphere. The intention for the model is primarily to simulate long-lived greenhouse gases and ozone-depleting substances. A major anticipated application is to infer emissions of these long-lived gases from measurements of atmospheric mole fractions.

The model is driven by monthly averaged transport, derived from MERRA-2 meteorology, and eddy transport derived from experiments using the GEOS-Chem 3D model. The model's zonal transport is generally comparable to GEOS-Chem, although its inter-

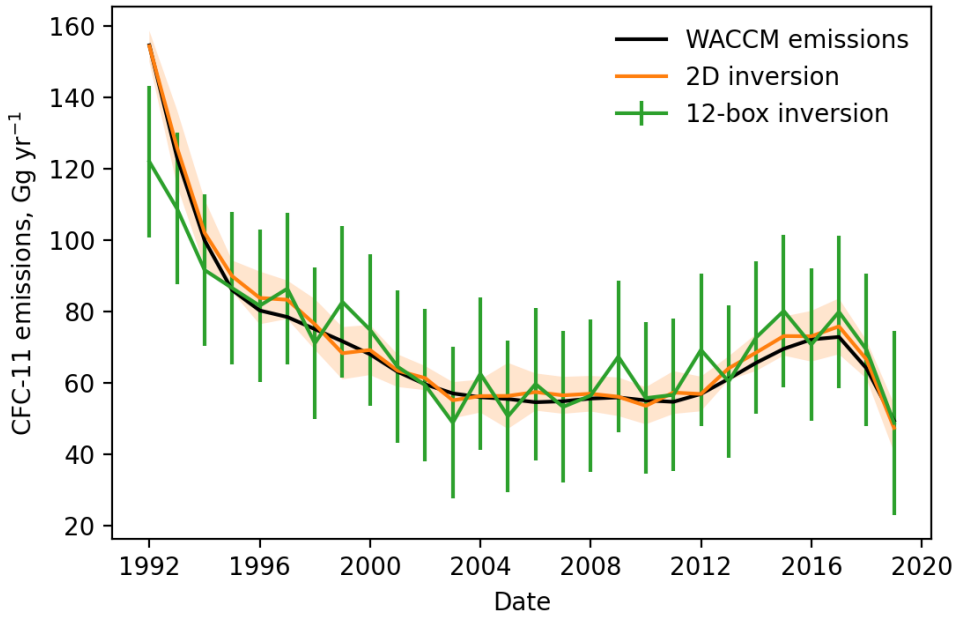

Figure 6. Emissions of CFC-11 from 1992-2019 estimated using the 2D model and mole fractions simulated using WACCM and an inverse framework. The orange line shows the mean global emissions estimated using the 2D model with the one standard deviation uncertainty shown by the shading. The black line shows the annual total emissions used in WACCM to simulate the mole fractions used as input to the inverse framework. Emissions derived using a 12-box model are also shown (green) with the error bars showing the one standard deviation uncertainty.

hemispheric transport appears to be slightly faster than both GEOS-Chem and that derived from measurements. Emissions derived with the 2D model from mole fractions simulated using a distinct 3D transport model, WACCM, are generally in good agreement with those used used as input to the WACCM forward simulation. A motivating factor for creating the model was to better simulate the influence of large-scale dynamics on surface mole fractions over existing simplified models, such as box models. The new 2D model produces a change to surface concentrations and throughout the middle atmosphere, which is qualitatively in phase with the QBO at 20 hPa.

The model is open-source and freely available. Transport parameters can be derived from different meteorological reanalysis and/or 3D models using an approach similar to that presented. The major intended use is in the estimation of long-lived trace gas emissions, although the investigation of many other processes is possible using the model, such as the study of dynamical transport.

6 Open Research

The 2D model, MALTA: Model of Averaged in Longitude Transport in the Atmosphere, is available on GitHub `https://github.com/lukewestern/malta` or L. Western (2023b, `https://doi.org/10.5281/zenodo.8097960`). GEOS-Chem 13.3.4 is available at The International GEOS-Chem User Community (2021, `https://doi.org/10.5281/zenodo.5764874`). The 12-box model and the inverse method used to quantify emissions are available via GitHub (`https://github.com/mrghg/py12box` and `https://github.com/mrghg/py12box_invert`) and Zenodo (Rigby and Western (2022b, `https://doi.org/10.5281/zenodo.6857447`), and Rigby and Western (2022a, `https://doi.org/10.5281/zenodo.6857794`)). The GEOS-Chem SF_6 outputs used for validation, scripts to generate the tracer fields using GEOS-Chem to derive the eddy-flux, and the script and data to quantify emissions of CFC-11 can be found at L. Western (2023a, `https://doi.org/10.5281/zenodo.8097547`).

Acknowledgments

Luke M. Western received funding from the European Union's Horizon 2020 research and innovation programme under Marie Skłodowska-Curie grant agreement no. 101030750. Matt Rigby is supported by the NERC Investigating HALocarbon impacts on the global Environment (InHALE) project, NE/X00452X/1.

References

Adcock, K. E., Fraser, P. J., Hall, B. D., Langenfelds, R. L., Lee, G., Montzka, S. A., ... Laube, J. C. (2021). Aircraft-Based Observations of Ozone-Depleting Substances in the Upper Troposphere and Lower Stratosphere in and Above the Asian Summer Monsoon. *Journal of Geophysical Research: Atmospheres*, *126*(1), e2020JD033137. Retrieved 2023-04-06, from `https://onlinelibrary.wiley.com/doi/abs/10.1029/2020JD033137` (_eprint: https://onlinelibrary.wiley.com/doi/pdf/10.1029/2020JD033137) doi: 10.1029/2020JD033137

Adcock, K. E., Reeves, C. E., Gooch, L. J., Leedham Elvidge, E. C., Ashfold, M. J., Brenninkmeijer, C. A. M., ... Laube, J. C. (2018, April). Continued increase of CFC-113a (CCl_3CF_3) mixing ratios in the global atmosphere: emissions, occurrence and potential sources. *Atmospheric Chemistry and Physics*, *18*(7), 4737–4751. Retrieved 2020-07-28, from `https://www.atmos-chem-phys.net/18/4737/2018/` doi: 10.5194/acp-18-4737-2018

Andrews, D. G., Holton, J. R., & Leovy, C. B. (1999). *Middle atmosphere dynamics* (3. print ed.) (No. 40). Orlando, Fla.: Acad. Pr.

Appenzeller, C., Holton, J. R., & Rosenlof, K. H. (1996). Seasonal variation of mass transport across the tropopause. *Journal of Geophysical Research: Atmospheres*, *101*(D10), 15071–15078. Retrieved 2023-04-03, from https://onlinelibrary.wiley.com/doi/abs/10.1029/96JD00821 (_eprint: https://onlinelibrary.wiley.com/doi/pdf/10.1029/96JD00821) doi: 10.1029/96JD00821

Arakawa, A., & Lamb, V. R. (1977). Computational Design of the Basic Dynamical Processes of the UCLA General Circulation Model. In *Methods in Computational Physics: Advances in Research and Applications* (Vol. 17, pp. 173–265). Elsevier. Retrieved 2023-03-09, from https://linkinghub.elsevier.com/retrieve/pii/B9780124608177500094 doi: 10.1016/B978-0-12-460817-7.50009-4

Bachman, S., & Fox-Kemper, B. (2013, April). Eddy parameterization challenge suite I: Eady spindown. *Ocean Modelling*, *64*, 12–28. Retrieved 2022-01-25, from https://www.sciencedirect.com/science/article/pii/S1463500312001801 doi: 10.1016/j.ocemod.2012.12.003

Bachman, S., Fox-Kemper, B., & Bryan, F. (2015, February). A tracer-based inversion method for diagnosing eddy-induced diffusivity and advection. *Ocean Modelling*, *86*, 1–14. Retrieved 2022-01-21, from https://linkinghub.elsevier.com/retrieve/pii/S1463500314001735 doi: 10.1016/j.ocemod.2014.11.006

Bachman, S. D., Fox-Kemper, B., & Bryan, F. O. (2020). A Diagnosis of Anisotropic Eddy Diffusion From a High-Resolution Global Ocean Model. *Journal of Advances in Modeling Earth Systems*, *12*(2), e2019MS001904. Retrieved 2023-03-09, from https://onlinelibrary.wiley.com/doi/abs/10.1029/2019MS001904 (_eprint: https://onlinelibrary.wiley.com/doi/pdf/10.1029/2019MS001904) doi: 10.1029/2019MS001904

Baldwin, M. P., Gray, L. J., Dunkerton, T. J., Hamilton, K., Haynes, P. H., Randel, W. J., ... Takahashi, M. (2001). The quasi-biennial oscillation. *Reviews of Geophysics*, *39*(2), 179–229. Retrieved 2022-06-30, from https://onlinelibrary.wiley.com/doi/abs/10.1029/1999RG000073 (_eprint: https://onlinelibrary.wiley.com/doi/pdf/10.1029/1999RG000073) doi: 10.1029/1999RG000073

Bey, I., Jacob, D. J., Yantosca, R. M., Logan, J. A., Field, B. D., Fiore, A. M., ... Schultz, M. G. (2001). Global modeling of tropospheric chemistry with assimilated meteorology: Model description and evaluation. *Journal of Geophysical Research: Atmospheres*, *106*(D19), 23073–23095. Retrieved 2023-03-09, from https://onlinelibrary.wiley.com/doi/abs/10.1029/2001JD000807 (_eprint: https://onlinelibrary.wiley.com/doi/pdf/10.1029/2001JD000807) doi: 10.1029/2001JD000807

Bratseth, A. M. (1998, January). On the estimation of transport characteristics of atmospheric data sets. *Tellus A: Dynamic Meteorology and Oceanography*, *50*(4), 451–467. Retrieved 2022-03-02, from https://www.tandfonline.com/doi/full/10.3402/tellusa.v50i4.14538 doi: 10.3402/tellusa.v50i4.14538

Burkholder, J., Sander, S., Abbatt, J., Barker, J., Cappa, C., Crounse, J., ... Wine, P. (2020). *Chemical kinetics and photochemical data for use in atmospheric studies; evaluation number 19.* Root. Retrieved from https://hdl.handle.net/2014/49199 (Edition: V1 Section: 2020-05-01 00:00:00.0)

Burkholder, J. B., & Hodnebrog, Ø. (2022). Appendix: Summary of Abundances, Lifetimes, ODPs, REs, GWPs, and GTPs. In *Scientific Assessment of Ozone Depletion: 2022.* Geneva, Switzerland: World Meteorological Organization. Retrieved from https://csl.noaa.gov/assessments/ozone/2022/downloads/2022OzoneAssessment.pdf

Butcher, J. C. (1996, March). A history of Runge-Kutta methods. *Applied Numerical Mathematics*, *20*(3), 247–260. Retrieved 2021-11-04, from https://www.sciencedirect.com/science/article/pii/0168927495001085 doi: 10.1016/0168-9274(95)00108-5

Carpenter, R. L., Droegemeier, K. K., Woodward, P. R., & Hane, C. E. (1990, March). Application of the Piecewise Parabolic Method (PPM) to Meteorological Modeling. *Monthly Weather Review*, *118*(3), 586–612. Retrieved 2023-03-09, from https://journals.ametsoc.org/view/journals/mwre/118/3/1520-0493_1990_118_0586_aotppm_2_0_co_2.xml (Publisher: American Meteorological Society Section: Monthly Weather Review) doi: 10.1175/1520-0493(1990)118⟨0586:AOTPPM⟩2.0.CO;2

Claxton, T., Hossaini, R., Wilson, C., Montzka, S. A., Chipperfield, M. P., Wild, O., ... Lunder, C. (2020). A Synthesis Inversion to Constrain Global Emissions of Two Very Short Lived Chlorocarbons: Dichloromethane, and Perchloroethylene. *Journal of Geophysical Research: Atmospheres*, *125*(12), e2019JD031818. Retrieved 2023-03-09, from https://onlinelibrary.wiley.com/doi/abs/10.1029/2019JD031818 (_eprint: https://onlinelibrary.wiley.com/doi/pdf/10.1029/2019JD031818) doi: 10.1029/2019JD031818

Colella, P., & Woodward, P. R. (1984, April). The Piecewise Parabolic Method (PPM) for gas-dynamical simulations. *Journal of Computational Physics*, *54*(1), 174–201. Retrieved 2022-05-17, from https://linkinghub.elsevier.com/retrieve/pii/0021999184901438 doi: 10.1016/0021-9991(84)90143-8

Cunnold, D. M., Prinn, R. G., Rasmussen, R. A., Simmonds, P. G., Alyea, F. N., Cardelino, C. A., ... Rosen, R. D. (1983). The Atmospheric Lifetime Experiment: 3. Lifetime methodology and application to three years of CFCl3 data. *Journal of Geophysical Research: Oceans*, *88*(C13), 8379–8400. Retrieved 2021-06-22, from https://agupubs.onlinelibrary.wiley.com/doi/abs/10.1029/JC088iC13p08379 (_eprint: https://agupubs.onlinelibrary.wiley.com/doi/pdf/10.1029/JC088iC13p08379) doi: 10.1029/JC088iC13p08379

du Toit, E., O'Brien, M., & Vann, R. (2018, July). Positivity-preserving scheme for two-dimensional advection–diffusion equations including mixed derivatives. *Computer Physics Communications*, *228*, 61–68. Retrieved 2023-01-17, from https://linkinghub.elsevier.com/retrieve/pii/S0010465518300766 doi: 10.1016/j.cpc.2018.03.004

Dutton, G., Hall, B., Dlugokencky, E., Lan, X., Nance, J., & Madronich, M. (2022). *Combined atmospheric sulfur hexaflouride dry air mole fractions from the noaa gml halocarbons sampling network, 1995-2022, version: 2022-10-07.* (Dataset) doi: 10.15138/TQ02-ZX42

Fleming, E. L., Newman, P. A., Liang, Q., & Daniel, J. S. (2020). The Impact of Continuing CFC-11 Emissions on Stratospheric Ozone. *Journal of Geophysical Research: Atmospheres*, *125*(3), e2019JD031849. Retrieved 2020-05-26, from https://agupubs.onlinelibrary.wiley.com/doi/abs/10.1029/2019JD031849 (_eprint: https://agupubs.onlinelibrary.wiley.com/doi/pdf/10.1029/2019JD031849) doi: 10.1029/2019JD031849

Gelaro, R., McCarty, W., Suárez, M. J., Todling, R., Molod, A., Takacs, L., ... Zhao, B. (2017, July). The Modern-Era Retrospective Analysis for Research and Applications, Version 2 (MERRA-2). *Journal of Climate*, *30*(14), 5419–5454. Retrieved 2023-03-09, from https://journals.ametsoc.org/doi/10.1175/JCLI-D-16-0758.1 doi: 10.1175/JCLI-D-16-0758.1

Gilliland, A. B., & Hartley, D. E. (1998). Interhemispheric transport and the role of convective parameterizations. *Journal of Geophysical Research: Atmospheres*, *103*(D17), 22039–22045. Retrieved 2023-04-06,

591 from https://onlinelibrary.wiley.com/doi/abs/10.1029/98JD01726
592 (_eprint: https://onlinelibrary.wiley.com/doi/pdf/10.1029/98JD01726) doi:
593 10.1029/98JD01726
594 Griffies, S. M. (1998, May). The Gent–McWilliams Skew Flux. *Jour-*
595 *nal of Physical Oceanography*, *28*(5), 831–841. Retrieved 2023-03-02,
596 from https://journals.ametsoc.org/view/journals/phoc/28/5/
597 1520-0485_1998_028_0831_tgmsf_2.0.co_2.xml (Publisher: American
598 Meteorological Society Section: Journal of Physical Oceanography) doi:
599 10.1175/1520-0485(1998)028⟨0831:TGMSF⟩2.0.CO;2
600 Hersbach, H., Bell, B., Berrisford, P., Hirahara, S., Horányi, A., Muñoz-Sabater, J.,
601 ... Thépaut, J.-N. (2020). The ERA5 global reanalysis. *Quarterly Journal*
602 *of the Royal Meteorological Society*, *146*(730), 1999–2049. Retrieved 2023-03-
603 17, from https://onlinelibrary.wiley.com/doi/abs/10.1002/qj.3803
604 (_eprint: https://onlinelibrary.wiley.com/doi/pdf/10.1002/qj.3803) doi:
605 10.1002/qj.3803
606 Holton, J. R. (1981). An advective model for two-dimensional trans-
607 port of stratospheric trace species. *Journal of Geophysical Research:*
608 *Oceans*, *86*(C12), 11989–11994. Retrieved 2023-05-26, from https://
609 onlinelibrary.wiley.com/doi/abs/10.1029/JC086iC12p11989 (_eprint:
610 https://onlinelibrary.wiley.com/doi/pdf/10.1029/JC086iC12p11989) doi:
611 10.1029/JC086iC12p11989
612 Hough, A. M. (1989, January). The development of a two-dimensional global tro-
613 pospheric model—1. The model transport. *Atmospheric Environment (1967)*,
614 *23*(6), 1235–1261. Retrieved 2022-03-02, from https://www.sciencedirect
615 .com/science/article/pii/0004698189901509 doi: 10.1016/0004-6981(89)
616 90150-9
617 Hu, L., Jacob, D. J., Liu, X., Zhang, Y., Zhang, L., Kim, P. S., ... Yantosca, R. M.
618 (2017, October). Global budget of tropospheric ozone: Evaluating recent
619 model advances with satellite (OMI), aircraft (IAGOS), and ozonesonde
620 observations. *Atmospheric Environment*, *167*, 323–334. Retrieved 2023-
621 04-03, from https://www.sciencedirect.com/science/article/pii/
622 S1352231017305484 doi: 10.1016/j.atmosenv.2017.08.036
623 Iwasaki, T. (1989). A Diagnostic Formulation for Wave-Mean Flow Interac-
624 tions and Lagrangian-Mean Circulation with a Hybrid Vertical Coordi-
625 nate of Pressure and Isentropes. *Journal of the Meteorological Society*
626 *of Japan. Ser. II*, *67*(2), 293–312. Retrieved 2023-06-01, from https://
627 www.jstage.jst.go.jp/article/jmsj1965/67/2/67_2_293/_article doi:
628 10.2151/jmsj1965.67.2_293
629 Janssens-Maenhout, G., Crippa, M., Guizzardi, D., Muntean, M., & Schaaf, E.
630 (2011). *Emissions database for global atmospheric research, version v4.2 (time-*
631 *series).* European Commission, Joint Research Centre (JRC). Retrieved
632 from http://data.europa.eu/89h/jrc-edgar-emissiontimeseriesv42
633 (Dataset)
634 Lam, S. K., Pitrou, A., & Seibert, S. (2015, November). Numba: a LLVM-based
635 Python JIT compiler. In *Proceedings of the Second Workshop on the LLVM*
636 *Compiler Infrastructure in HPC* (pp. 1–6). New York, NY, USA: Association
637 for Computing Machinery. Retrieved 2023-06-01, from https://dl.acm.org/
638 doi/10.1145/2833157.2833162 doi: 10.1145/2833157.2833162
639 Laube, J. C., Mohd Hanif, N., Martinerie, P., Gallacher, E., Fraser, P. J., Langen-
640 felds, R., ... Oram, D. E. (2016, December). Tropospheric observations of
641 CFC-114 and CFC-114a with a focus on long-term trends and emissions. *At-*
642 *mospheric Chemistry and Physics*, *16*(23), 15347–15358. Retrieved 2022-06-30,
643 from https://acp.copernicus.org/articles/16/15347/2016/ (Publisher:
644 Copernicus GmbH) doi: 10.5194/acp-16-15347-2016
645 Laube, J. C., Tegtmeier, S., Fernandez, R. P., Harrison, J., Hu, L., Krummel, P., ...

Western, L. (2023). Update on ozone-depleting substances (odss) and other gases of interest to the montreal protocol. *978-9914-733-97-6*.

Lin, S.-J., Chao, W. C., Sud, Y. C., & Walker, G. K. (1994, July). A Class of the van Leer-type Transport Schemes and Its Application to the Moisture Transport in a General Circulation Model. *Monthly Weather Review*, *122*(7), 1575–1593. Retrieved 2023-03-09, from http://journals.ametsoc.org/doi/10.1175/1520-0493(1994)122<1575:ACOTVL>2.0.CO;2 doi: 10.1175/1520-0493(1994)122⟨1575:ACOTVL⟩2.0.CO;2

Lin, S.-J., & Rood, R. B. (1996, September). Multidimensional Flux-Form Semi-Lagrangian Transport Schemes. *Monthly Weather Review*, *124*(9), 2046–2070. Retrieved 2022-04-15, from http://journals.ametsoc.org/doi/10.1175/1520-0493(1996)124<2046:MFFSLT>2.0.CO;2 doi: 10.1175/1520-0493(1996)124⟨2046:MFFSLT⟩2.0.CO;2

Lintner, B. R., Gilliland, A. B., & Fung, I. Y. (2004). Mechanisms of convection-induced modulation of passive tracer interhemispheric transport interannual variability. *Journal of Geophysical Research: Atmospheres*, *109*(D13). Retrieved 2023-04-06, from https://onlinelibrary.wiley.com/doi/abs/10.1029/2003JD004306 (_eprint: https://onlinelibrary.wiley.com/doi/pdf/10.1029/2003JD004306) doi: 10.1029/2003JD004306

Lunt, M. F., Rigby, M., Ganesan, A. L., Manning, A. J., Prinn, R. G., O'Doherty, S., ... Simmonds, P. G. (2015, May). Reconciling reported and unreported HFC emissions with atmospheric observations. *Proceedings of the National Academy of Sciences*, *112*(19), 5927–5931. Retrieved 2018-10-29, from http://www.pnas.org/lookup/doi/10.1073/pnas.1420247112 doi: 10.1073/pnas.1420247112

Marsh, D. R., Mills, M. J., Kinnison, D. E., Lamarque, J.-F., Calvo, N., & Polvani, L. M. (2013, October). Climate Change from 1850 to 2005 Simulated in CESM1(WACCM). *Journal of Climate*, *26*(19), 7372–7391. Retrieved 2023-03-17, from https://journals.ametsoc.org/view/journals/clim/26/19/jcli-d-12-00558.1.xml (Publisher: American Meteorological Society Section: Journal of Climate) doi: 10.1175/JCLI-D-12-00558.1

Montzka, S. A., Dutton, G. S., Portmann, R. W., Chipperfield, M. P., Davis, S., Feng, W., ... Theodoridi, C. (2021, February). A decline in global CFC-11 emissions during 2018-2019. *Nature*, *590*(7846), 428–432. Retrieved 2022-06-30, from https://www.nature.com/articles/s41586-021-03260-5 (Number: 7846 Publisher: Nature Publishing Group) doi: 10.1038/s41586-021-03260-5

Montzka, S. A., Dutton, G. S., Yu, P., Ray, E., Portmann, R. W., Daniel, J. S., ... Elkins, J. W. (2018, May). An unexpected and persistent increase in global emissions of ozone-depleting CFC-11. *Nature*, *557*(7705), 413–417. Retrieved 2018-08-30, from http://www.nature.com/articles/s41586-018-0106-2 doi: 10.1038/s41586-018-0106-2

Murray, L. T., Jacob, D. J., Logan, J. A., Hudman, R. C., & Koshak, W. J. (2012). Optimized regional and interannual variability of lightning in a global chemical transport model constrained by LIS/OTD satellite data. *Journal of Geophysical Research: Atmospheres*, *117*(D20). Retrieved 2023-03-10, from https://onlinelibrary.wiley.com/doi/abs/10.1029/2012JD017934 (_eprint: https://onlinelibrary.wiley.com/doi/pdf/10.1029/2012JD017934) doi: 10.1029/2012JD017934

Mühle, J., Kuijpers, L. J. M., Stanley, K. M., Rigby, M., Western, L. M., Kim, J., ... Weiss, R. F. (2022, March). Global emissions of perfluorocyclobutane (PFC-318, <i>c</i>-C₄F₈) resulting from the use of hydrochlorofluorocarbon-22 (HCFC-22) feedstock to produce

polytetrafluoroethylene (PTFE) and related fluorochemicals. *Atmospheric Chemistry and Physics*, *22*(5), 3371–3378. Retrieved 2023-06-27, from https://acp.copernicus.org/articles/22/3371/2022/ doi: 10.5194/acp-22-3371-2022

Newland, M. J., Reeves, C. E., Oram, D. E., Laube, J. C., Sturges, W. T., Hogan, C., ... Fraser, P. J. (2013, June). Southern hemispheric halon trends and global halon emissions, 1978–2011. *Atmospheric Chemistry and Physics*, *13*(11), 5551–5565. Retrieved 2021-06-22, from https://acp.copernicus.org/articles/13/5551/2013/ doi: 10.5194/acp-13-5551-2013

Newman, P. A., Coy, L., Pawson, S., & Lait, L. R. (2016). The anomalous change in the QBO in 2015–2016. *Geophysical Research Letters*, *43*(16), 8791–8797. Retrieved 2023-03-17, from https://onlinelibrary.wiley.com/doi/abs/10.1002/2016GL070373 (_eprint: https://onlinelibrary.wiley.com/doi/pdf/10.1002/2016GL070373) doi: 10.1002/2016GL070373

Newman, P. A., Oman, L. D., Douglass, A. R., Fleming, E. L., Frith, S. M., Hurwitz, M. M., ... Velders, G. J. M. (2009, March). What would have happened to the ozone layer if chlorofluorocarbons (CFCs) had not been regulated? *Atmospheric Chemistry and Physics*, *9*(6), 2113–2128. Retrieved 2022-06-30, from https://acp.copernicus.org/articles/9/2113/2009/ (Publisher: Copernicus GmbH) doi: 10.5194/acp-9-2113-2009

Orbe, C., Yang, H., Waugh, D. W., Zeng, G., Morgenstern, O., Kinnison, D. E., ... Banerjee, A. (2018, May). Large-scale tropospheric transport in the Chemistry–Climate Model Initiative (CCMI) simulations. *Atmospheric Chemistry and Physics*, *18*(10), 7217–7235. Retrieved 2023-06-26, from https://acp.copernicus.org/articles/18/7217/2018/ (Publisher: Copernicus GmbH) doi: 10.5194/acp-18-7217-2018

Park, S., Western, L. M., Saito, T., Redington, A. L., Henne, S., Fang, X., ... Rigby, M. (2021, February). A decline in emissions of CFC-11 and related chemicals from eastern China. *Nature*, *590*(7846), 433–437. Retrieved 2021-05-18, from https://www.nature.com/articles/s41586-021-03277-w (Number: 7846 Publisher: Nature Publishing Group) doi: 10.1038/s41586-021-03277-w

Patra, P. K., Takigawa, M., Dutton, G. S., Uhse, K., Ishijima, K., Lintner, B. R., ... Elkins, J. W. (2009, February). Transport mechanisms for synoptic, seasonal and interannual SF_6 variations and "age" of air in troposphere. *Atmospheric Chemistry and Physics*, *9*(4), 1209–1225. Retrieved 2023-04-03, from https://acp.copernicus.org/articles/9/1209/2009/ (Publisher: Copernicus GmbH) doi: 10.5194/acp-9-1209-2009

Pimlott, M. A., Pope, R. J., Kerridge, B. J., Latter, B. G., Knappett, D. S., Heard, D. E., ... Chipperfield, M. P. (2022, August). Investigating the global OH radical distribution using steady-state approximations and satellite data. *Atmospheric Chemistry and Physics*, *22*(16), 10467–10488. Retrieved 2023-03-09, from https://acp.copernicus.org/articles/22/10467/2022/ (Publisher: Copernicus GmbH) doi: 10.5194/acp-22-10467-2022

Plumb, R. A. (1979, September). Eddy Fluxes of Conserved Quantities by Small-Amplitude Waves. *Journal of the Atmospheric Sciences*, *36*(9), 1699–1704. Retrieved 2023-03-02, from https://journals.ametsoc.org/view/journals/atsc/36/9/1520-0469_1979_036_1699_efocqb_2_0_co_2.xml (Publisher: American Meteorological Society Section: Journal of the Atmospheric Sciences) doi: 10.1175/1520-0469(1979)036⟨1699:EFOCQB⟩2.0.CO;2

Plumb, R. A., & Mahlman, J. D. (1987, January). The Zonally Averaged Transport Characteristics of the GFDL General Circulation/Transport Model. *Journal of the Atmospheric Sciences*, *44*(2), 298–327. Retrieved 2021-11-09, from https://journals.ametsoc.org/view/journals/atsc/44/2/

1520-0469_1987_044_0298_tzatco_2_0_co_2.xml (Publisher: American Meteorological Society Section: Journal of the Atmospheric Sciences) doi: 10.1175/1520-0469(1987)044⟨0298:TZATCO⟩2.0.CO;2

Ray, E. A., Portmann, R. W., Yu, P., Daniel, J., Montzka, S. A., Dutton, G. S., ... Rosenlof, K. H. (2020, January). The influence of the stratospheric Quasi-Biennial Oscillation on trace gas levels at the Earth's surface. *Nature Geoscience*, *13*(1), 22–27. Retrieved 2020-04-28, from http://www.nature.com/articles/s41561-019-0507-3 doi: 10.1038/s41561-019-0507-3

Rigby, M., Prinn, R. G., O'Doherty, S., Montzka, S. A., McCulloch, A., Harth, C. M., ... Fraser, P. J. (2013, March). Re-evaluation of the lifetimes of the major CFCs and CH_3CCl_3 using atmospheric trends. *Atmospheric Chemistry and Physics*, *13*(5), 2691–2702. Retrieved 2021-06-22, from https://acp.copernicus.org/articles/13/2691/2013/ (Publisher: Copernicus GmbH) doi: 10.5194/acp-13-2691-2013

Rigby, M., & Western, L. (2022a, July). *mrghg/py12box_invert: v0.0.2.* Zenodo. Retrieved 2023-06-30, from https://zenodo.org/record/6857794 doi: 10.5281/ZENODO.6857794

Rigby, M., & Western, L. (2022b, July). *mrghg/py12box: v0.2.1.* Zenodo. Retrieved 2023-06-30, from https://zenodo.org/record/6857447 doi: 10.5281/ZENODO.6857447

Ruiz, D. J., Prather, M. J., Strahan, S. E., Thompson, R. L., Froidevaux, L., & Steenrod, S. D. (2021). How Atmospheric Chemistry and Transport Drive Surface Variability of N2O and CFC-11. *Journal of Geophysical Research: Atmospheres*, *126*(8), e2020JD033979. Retrieved 2022-06-30, from https://onlinelibrary.wiley.com/doi/abs/10.1029/2020JD033979 (_eprint: https://onlinelibrary.wiley.com/doi/pdf/10.1029/2020JD033979) doi: 10.1029/2020JD033979

Shine, K. (1989). Sources and sinks of zonal momentum in the middle atmosphere diagnosed using the diabatic circulation. *Quarterly Journal of the Royal Meteorological Society*, *115*(486), 265–292. Retrieved 2023-03-09, from https://onlinelibrary.wiley.com/doi/abs/10.1002/qj.49711548604 (_eprint: https://onlinelibrary.wiley.com/doi/pdf/10.1002/qj.49711548604) doi: 10.1002/qj.49711548604

Simmonds, P. G., Rigby, M., Manning, A. J., Park, S., Stanley, K. M., McCulloch, A., ... Prinn, R. G. (2020, June). The increasing atmospheric burden of the greenhouse gas sulfur hexafluoride (SF_6). *Atmospheric Chemistry and Physics*, *20*(12), 7271–7290. Retrieved 2023-03-20, from https://acp.copernicus.org/articles/20/7271/2020/ (Publisher: Copernicus GmbH) doi: 10.5194/acp-20-7271-2020

Stanley, K. M., Say, D., Mühle, J., Harth, C. M., Krummel, P. B., Young, D., ... Rigby, M. (2020, January). Increase in global emissions of HFC-23 despite near-total expected reductions. *Nature Communications*, *11*(1), 1–6. Retrieved 2020-03-10, from https://www.nature.com/articles/s41467-019-13899-4 (Number: 1 Publisher: Nature Publishing Group) doi: 10.1038/s41467-019-13899-4

Strand, A., & Hov, Ø. (1993). A two-dimensional zonally averaged transport model including convective motions and a new strategy for the numerical solution. *Journal of Geophysical Research: Atmospheres*, *98*(D5), 9023–9037. Retrieved 2021-11-09, from https://onlinelibrary.wiley.com/doi/abs/10.1029/93JD00201 (_eprint: https://onlinelibrary.wiley.com/doi/pdf/10.1029/93JD00201) doi: 10.1029/93JD00201

Tarantola, A. (2005). *Inverse problem theory and methods for model parameter estimation.* Philadelphia, PA: Society for Industrial and Applied Mathematics. (OCLC: ocm56672375)

The International GEOS-Chem User Community. (2021, December). *geoschem/GCClassic: GEOS-Chem 13.3.4.* Zenodo. Retrieved 2023-03-09, from https://zenodo.org/record/5764874 doi: 10.5281/ZENODO.5764874

Tung, K. K. (1982, October). On the Two-Dimensional Transport of Stratospheric Trace Gases in Isentropic Coordinates. *Journal of the Atmospheric Sciences*, *39*(10), 2330–2355. Retrieved 2023-06-01, from https://journals.ametsoc.org/view/journals/atsc/39/10/1520-0469_1982_039_2330_ottdto_2_0_co_2.xml (Publisher: American Meteorological Society Section: Journal of the Atmospheric Sciences) doi: 10.1175/1520-0469(1982)039⟨2330:OTTDTO⟩2.0.CO;2

Waugh, D. W., Crotwell, A. M., Dlugokencky, E. J., Dutton, G. S., Elkins, J. W., Hall, B. D., ... Sweeney, C. (2013). Tropospheric SF6: Age of air from the Northern Hemisphere midlatitude surface. *Journal of Geophysical Research: Atmospheres*, *118*(19), 11,429–11,441. Retrieved 2023-04-15, from https://onlinelibrary.wiley.com/doi/abs/10.1002/jgrd.50848 (_eprint: https://onlinelibrary.wiley.com/doi/pdf/10.1002/jgrd.50848) doi: 10.1002/jgrd.50848

Western, L. (2023a, June). *Auxiliary files and data to generate eddy flux and validate 2D model for MALTA.* Zenodo. Retrieved 2023-06-30, from https://zenodo.org/record/8097547 doi: 10.5281/ZENODO.8097547

Western, L. (2023b, June). *lukewestern/malta: malta v0.1.2.* Zenodo. Retrieved 2023-06-30, from https://zenodo.org/record/8097960 doi: 10.5281/ZENODO.8097960

Western, L. M., Vollmer, M. K., Krummel, P. B., Adcock, K. E., Crotwell, M., Fraser, P. J., ... Laube, J. C. (2023, April). Global increase of ozone-depleting chlorofluorocarbons from 2010 to 2020. *Nature Geoscience*, *16*(4), 309–313. Retrieved 2023-06-27, from https://www.nature.com/articles/s41561-023-01147-w doi: 10.1038/s41561-023-01147-w

World Meteorological Organization (WMO). (2022). *Scientific Assessment of Ozone Depletion: 2022* (Tech. Rep. No. GAW Report No. 278). Geneva: Author.

Yang, H., Waugh, D. W., Orbe, C., Patra, P. K., Jöckel, P., Lamarque, J.-F., ... Dlugokencky, E. J. (2019). Evaluating Simulations of Interhemispheric Transport: Interhemispheric Exchange Time Versus SF6 Age. *Geophysical Research Letters*, *46*(2), 1113–1120. Retrieved 2023-03-29, from https://onlinelibrary.wiley.com/doi/abs/10.1029/2018GL080960 (_eprint: https://onlinelibrary.wiley.com/doi/pdf/10.1029/2018GL080960) doi: 10.1029/2018GL080960

Yu, K., Keller, C. A., Jacob, D. J., Molod, A. M., Eastham, S. D., & Long, M. S. (2018, January). Errors and improvements in the use of archived meteorological data for chemical transport modeling: an analysis using GEOS-Chem v11-01 driven by GEOS-5 meteorology. *Geoscientific Model Development*, *11*(1), 305–319. Retrieved 2023-03-20, from https://gmd.copernicus.org/articles/11/305/2018/ (Publisher: Copernicus GmbH) doi: 10.5194/gmd-11-305-2018

Zhuang, J., Dussin, R., Jüling, A., & Rasp, S. (2020, March). *JiaweiZhuang/xESMF: v0.3.0 Adding ESMF.LocStream capabilities.* Zenodo. Retrieved 2023-03-09, from https://zenodo.org/record/3700105 doi: 10.5281/ZENODO.3700105